

Conf. 770125--9

LA-UR -79-103

TITLE: DISPLACEMENT FUNCTIONS FOR DIATOMIC MATERIALS

AUTHOR(S): Don M. Parkin
C. Alton Coulter


SUBMITTED TO: First Topical Meeting on Fusion Reactor Materials
Jan 29-31, 1979, Miami Beach Florida

NOTICE

This report was prepared as an account of work sponsored by the United States Government. Neither the United States nor the United States Department of Energy, nor any of their employees, nor any of their contractors, subcontractors, or their employees, make any warranty, express or implied, or assumes any liability for the accuracy, completeness, or usefulness of any information, apparatus, or method disclosed, or represents that it would not infringe privately owned rights. Reproduction and distribution of this report are unlimited.

By acceptance of this article, the publisher recognizes that the U.S. Government retains a non-exclusive, royalty free license to publish or reproduce the published form of this contribution, or to allow others to do so, for U.S. Government purposes.

The Los Alamos Scientific Laboratory requests that the publisher identify this article as work performed under the auspices of the Department of Energy.


Los Alamos
Scientific Laboratory
of the University of California
LOS ALAMOS, NEW MEXICO 87545

An Affirmative Action/Equal Opportunity Employer

Form No. 836 R2
SL No. 2629
1/78

DEPARTMENT OF ENERGY
CONTRACT W-7405-ENG. 38

MASTER

DISPLACEMENT FUNCTIONS FOR DIATOMIC MATERIALS*

D. M. PARKIN AND C. A. COULTER†

University of California, Los Alamos Scientific
Laboratory, Los Alamos, New Mexico 87545

We have used an extension of the methods of Lindhard et al. to calculate the total displacement function $n_{ij}(E)$ for a number of diatomic materials, where $n_{ij}(E)$ is defined to be the average number of atoms of type j which are displaced from their sites in a displacement cascade initiated by a PKA of type i and energy E . From the $n_{ij}(E)$ one can calculate the fraction $\eta_{ij}(E)$ of the displacements produced by a type i PKA with energy E which are of type j . Values of the η_{ij} for MgO, CaO, Al₂O₃, and TaO are presented. It is shown that for diatomic materials with mass ratios reasonably near one (e.g., MgO, Al₂O₃) and equal displacement thresholds for the two species the η_{ij} become independent of the PKA type i at energies only a few times threshold. However, for larger mass ratios the η_{ij} do not become independent of i until much larger energies are reached - e.g. $> 10^5$ eV for TaO. In addition, it is found that the η_{ij} depend sensitively on the displacement thresholds, with very dramatic changes occurring when the two thresholds become significantly different from one another.

1. INTRODUCTION

A process of central importance in the study of radiation damage effects in solids is the displacement cascade occurring when an atom in a solid material is displaced from its lattice site by an incident damaging particle and move through the material producing additional displacements. Polyatomic materials such as alloys, insulators, and ceramics play significant roles in many fusion reactor designs. Theoretical damage functions that describe displacement cascades in these materials, such as are available for monatomic materials, have been lacking. Damage functions are needed which can provide an estimate of the performance of these materials under fusion conditions by extrapolation from accessible experimental situations.

Using various approximations, several authors have investigated aspects of displacement cascades in polyatomic materials. The work of Baroody [1], Andersen and Sigmund [2], and Matsutani and Ishino [3] is of particular interest for the present discussion. Baroody assumed hard-sphere scattering, no electronic energy loss, and the same displacement threshold for each atom type, but allowed each atom type to have a different mass. His primary conclusion relevant to this discussion is that the number of type- i atoms displaced depends only weakly on the mass of atom i . Andersen and Sigmund, using power-law cross sections, neglecting electronic energy loss in all actual calculations, and employing approximate solution methods, integrated their recoil density to obtain a

displacement function for diatomic materials.

Their calculations were aimed at recoil energies in the keV range and the case of widely different masses of the constituent atoms. They gave an approximate expression for a displacement function in which the number of type- j displacements depends only on the energy of the PKA and not its type. Matsutani and Ishino calculated damage energies deposited in TaO by a number of projectile atoms. They determined the division of deposited energy between the Ta and O sublattices using two different hypotheses concerning the manner in which this division is made.

The results presented in this paper are a small part of a larger set of calculations [4,5] aimed at developing a set of functions describing displacement cascades in polyatomic materials. The calculations, based on the work of Lindhard et al., [6-8] use the simplest of binary collision approximations in which the material is assumed to be random and amorphous and no simultaneous collisions of more than two atoms are considered. Our method proceeds by extending the basic integrodifferential equation of Lindhard et al. to determine functions which give direct information about atomic displacements as functions of PKA energy and type stoichiometry, atomic masses, displacement thresholds and binding energies for each atom type, and capture (or replacement) thresholds for each pair of atom types. One such function, the total displacement function, is defined in the next section; and certain of its properties for various diatomic materials are discussed in the remainder of the paper.

* Research supported by the U. S. Department of Energy

† Permanent address Department of Physics, The University of Alabama, University, Alabama

II. THEORY OF THE TOTAL DISPLACEMENT FUNCTION

The total displacement function $n_{ij}(E)$ is defined to be the average number of type- j atoms which are at any time displaced from their sites in a displacement cascade initiated by a PKA of type i and initial energy E , with the convention that $n_{ij}(E)$ counts the PKA itself. The formulation of the equation for $n_{ij}(E)$ is most conveniently carried out in terms of $\bar{n}_{ij} \equiv n_{ij} - \delta_{ij}$. The function $\bar{n}_{ij}(E)$ is the number of type- j atoms displaced other than the PKA (though for the case of external bombardment by self-ions, $\bar{n}_{ij}(E)$ itself is the total number of displaced atoms of type i).

In deriving the integrodifferential equation for $\bar{n}_{ij}(E)$, it is convenient to make the following definitions: (1) the specific electronic stopping power (electronic energy loss per unit length per unit atom number density) for a moving atom of type i and energy E is denoted by $s_i(E)$; (2) the probability that an initially bound atom of type j which receives kinetic energy T in a collision will be displaced from its site as a consequence is indicated by $p_j(T)$; (3) the binding energy which the type- j atom loses to potential energy and/or in elastic processes as it is displaced from its site is represented by E_{ij}^b and (4) the probability that a type- i atom left with energy E after displacing a type- j atom will be trapped in the type- j site is denoted by $\lambda_{ij}(E)$. Finally, the symbol M_{ij} is used for the kinematic energy transfer efficiency $4A_i A_j / (A_i + A_j)^2$ for a collision of two atoms of types i and j . Using the method of Ref. 6, one obtains for $\bar{n}_{ij}(E)$ the equation

$$s_i(E) \bar{n}_{ij}(E) = \sum_k f_k \int_0^E M_{ik} \frac{d\sigma_{ik}(E, T)}{dT} \times \{p_k(T) [\delta_{kj} + \bar{n}_{kj}(T - E_k^b)] + [1 - p_k(T) \lambda_{ik}(E - T)] \bar{n}_{ij}(E - T) - n_{ij}(E)\}. \quad (1)$$

$\bar{n}_{ij}'(E)$ is the derivative of $\bar{n}_{ij}(E)$, where f_k is the atomic fraction of type- k atoms, and

$$\frac{d\sigma_{ik}(E, T)}{dT}$$

is the differential collision cross section for atoms of types i and k . In the calculations discussed below the collision cross section and electronic stopping power expressions of Lindhard et al. were used [7,8]. In addition, it was assumed that

$$p_k(T) = \begin{cases} 0, & T < E_k^d \\ 1, & T > E_k^d \end{cases} \quad (2)$$

$$\lambda_{ik}(E) = \begin{cases} 1, & E < E_{ik}^{\text{cap}} \\ 0, & E > E_{ik}^{\text{cap}} \end{cases} \quad (3)$$

where E_k^d is the displacement threshold for a type- k atom and E_{ik}^{cap} is the capture threshold for a type- i atom in a type- j site, defined to be the limiting residual energy of a type- i atom after it has displaced a type- k atom below which it will be trapped in the type- k site. In the calculations described below it was assumed that $E_i^d = 0$, that $E_{ik}^{\text{cap}} = E_i^d$, and that $E_{ik}^{\text{cap}} = (\sum E_i^d)/2$ for $i \neq k$. The dependence of $\bar{n}_{ij}(E)$ on the E_{ik}^{cap} for $i \neq k$ is in any case quite small for all physically reasonable values of E_{ik}^{cap} .

One of the important damage parameters for insulations and ceramics is the distribution of damage among the various sublattices of atomic type. The fraction of the total displacements produced by a PKA of type i which are of type j , excluding the PKA, is

$$\eta_{ij} \equiv \frac{\bar{n}_{ij}}{\sum_k \bar{n}_{ik}} \quad (4)$$

The parameter η_{ij} describes how the initial PKA energy becomes distributed on the sublattices as displacement. The following section discusses the values of η_{ij} which we have calculated for a number of materials.

III. RESULTS FOR DIATOMIC MATERIALS

Calculations of the total displacement function n_{ij} have been made using parameters appropriate for TaO, Al₂O₃, MgO, and CaO. For these materials we have examined the role of mass ratio and of the magnitude of the displacement threshold, as well as the effect of having equal vs. unequal displacement thresholds for the two atomic species. The results of these calculations are discussed below as representing typical cases, but they should not be interpreted as indicating the full range of effects which can be found in diatomic materials. In fact, the results given here plus many other calculations we have performed show that the inter-related roles of energy, atomic masses, binding energies, displacement and capture thresholds, and stoichiometry make derivation of completely general conclusions about displacement thresholds in polyatomic materials extremely difficult.

The simplest case to consider is that of a mass ratio near one and equal displacement thresholds. Measurements of the displacement thresholds for Mg and O in MgO have shown them to be similar: Chen et al. [9] measured the threshold for oxygen to be 60 eV, and Sharp and Rumsby [10] measured that for magnesium to be 64 ± 2 eV. Figure 1 shows values of η_{ij} for MgO which we have calculated assuming $E_{Mg}^d = E_O^d = 62$ eV. Near threshold it is seen

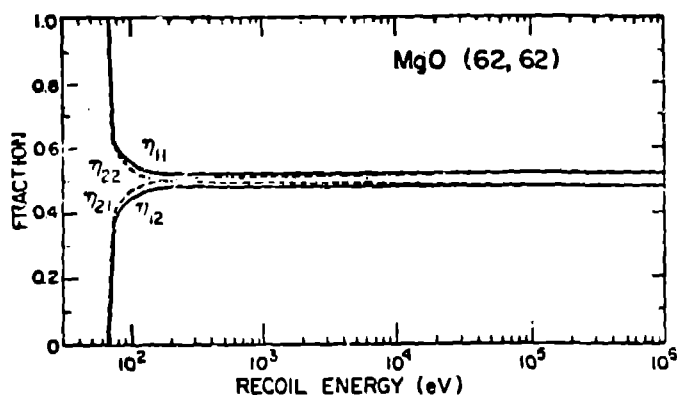


Fig. 1. The fraction η_{ij} of type-j displacements produced by a PKA of type i in MgO ($Mg = 1, O = 2$) assuming $E_1^d = E_2^d = 62$ eV.

that all displacements are on the sublattice of atoms of the same type as the PKA, as is required by kinematics. At energies only a few times this threshold, however, there is a uniform distribution of displacements between the two sublattices. In fact for $E \sim 4 E_j^d$, $\eta_{ij} \sim \eta_j$ (independent of i). Thus the fraction of type-j displacements becomes independent of PKA type for energies not too far above threshold, and $\eta_1 > \eta_2$ in this range. Experimental measurements of displacement thresholds in Al_2O_3 indicate that aluminum and oxygen ions have different threshold energies in this material. Compton and Arnold [11] measured a threshold energy that corresponded to either ~ 40 eV for aluminum or ~ 70 eV for oxygen. Phillips [12] has suggested that the thresholds are 18 eV for Al and 72 eV for O. We present results for two sets of calculations for Al_2O_3 . In Fig. 2 we have assumed $E_1^d = E_2^d = 60$ eV, similarly to the case of MgO; and we have used Phillips values in Fig. 3. The equal-threshold results for Al_2O_3 shown in Fig. 2 are very similar to those for

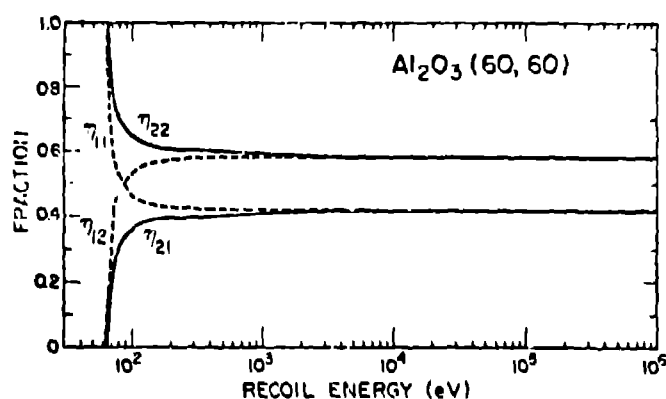


Fig. 2. The fraction η_{ij} of type-j displacements produced by a PKA of type i in Al_2O_3 ($Al = 1, O = 2$) assuming $E_1^d = E_2^d = 60$ eV.

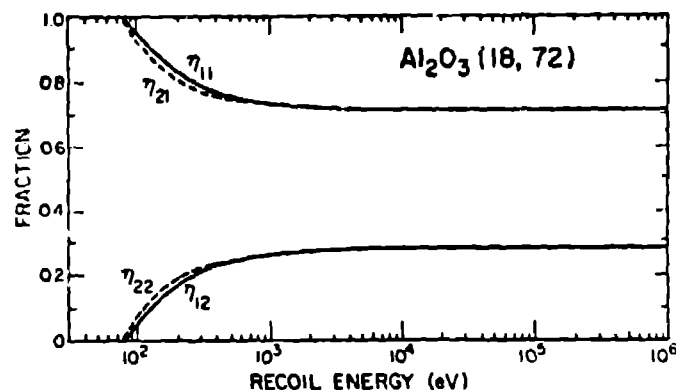


Fig. 3. The fraction η_{ij} of type-j displacements produced by a PKA of type i in Al_2O_3 ($Al = 1, O = 2$) assuming $E_1^d = 18$ eV, $E_2^d = 72$ eV.

MgO in Fig. 1, with one important exception: the relative magnitudes of the η_{ij} are reversed, and $\eta_2 > \eta_1$. Examination of the values of η_{ij} shows that this behavior can be explained by the difference in stoichiometry. However, the Al_2O_3 results for unequal displacement thresholds in Fig. 3 show a very different behavior than those of the equal-threshold case of Fig. 2. An oxygen PKA receiving energy at its displacement threshold can easily displace aluminum atoms. As a result, it displaces more aluminum atoms than oxygen atoms, and $\eta_{21} \rightarrow 1$ and correspondingly $\eta_{22} \rightarrow 0$ at threshold. The larger fraction of displacements is now associated with the atom with the lower threshold energy, not the atom of higher mass or atomic fraction.

For energies high enough so that $\eta_{ij} \sim \eta_j$ in Figs. 2 and 3 it is found that the $\eta_{ij}(E)$ scale rather closely as E_j^d , and consequently ratios of the η_i scale approximately as ratios of displacement thresholds.

TaO is a case of a material with rather widely different masses of the constituent atoms. Calculated results for TaO assuming $E_1^d = E_2^d = 60$ eV are given in Fig. 4. The fact that no displacements can occur on the type-j sublattice for type i PKA's until $E \geq E_j^d/M_{ij}$, or 201 eV for $i \neq j$, is clearly seen. The most striking feature of these results is that only at very high energies ($E > 10^5$ eV) is it reasonable to consider that $\eta_{ij} \sim \eta_j$.

To illustrate the effect of a change in the magnitude of the displacement threshold, results are shown for TaO in Fig. 5 with $E_1^d = E_2^d = 1$ eV. By comparison with Fig. 4 it is seen that the strong energy dependence of η_{ij} for TaO is only weakly affected by the value of the E_j^d . Also given in Fig. 5 are the results of Matsuani and Ishino [3] for the damage energy fractions in TaO . They display the same qualitative behavior as our results, and lie within the range

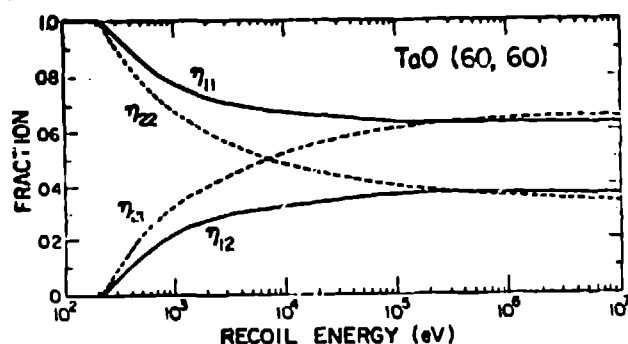


Fig. 4. The fraction η_{ij} of type-j displacements produced by a PKA of type i in TaO ($T_a = 1, O = 2$) assuming $E_1^d = E_2^d = 60$ eV.

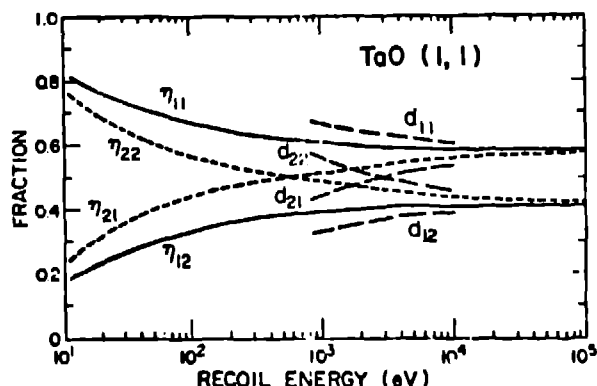


Fig. 5. The fraction η_{ij} of type-j displacements produced by a PKA of type i in TaO ($T_a = 1, O = 2$) assuming $E_1^d = E_2^d = 1$ eV, and the fractional damage energy d_{ij} for TaO from Ref 3.

of values of our η_{ij} obtained for the two different displacement thresholds.

A summary of results for the η_{ij} at $E = 10^7$ eV is given in the Table for several materials and sets of displacement threshold. It can be seen that for the equal-displacement threshold case the high energy values of the η_{ij} are only weakly dependent on mass ratio. This result is consistent with the conclusion of Baroody (1) mentioned earlier, though it should be noted again that he assumed hard-sphere scattering and neglected electronic energy loss while our results use more realistic cross sections and include electronic energy loss.

The three cases given for TaO show that the limiting values of η_{ij} are only weakly dependent on the value of the E_j^d , with a factor of 10^3 change in E_j^d altering the η_{ij} by only 20-40 %. Clearly this dependence should not be important for small changes in E_j^d . It is found that for energies large enough so that $\eta_{ij} \approx \eta_j$

Table 1
Values of η_{ij} For Several Materials and Threshold Energies

η_{11}	η_{12}	η_{21}	η_{22}
TaO (1, 1)			
0.58	0.42	0.59	0.41
TaO (60,60)			
0.63	0.37	0.66	0.34
TaO (1000,1000)			
0.71	0.29	0.73	0.27

Al ₂ O ₃ (18,72)			
0.73	0.27	0.73	0.27
Al ₂ O ₃ (60,60)			
0.42	0.58	0.42	0.58
Al ₂ O ₃ (72,18)			
0.16	0.84	0.16	0.84

MgO (62,62)			
0.52	0.48	0.52	0.48

CaO (60,60)			
0.55	0.45	0.55	0.45

the $\eta_{ij}(E)$ scale less well with E_j^d than in the case of Al₂O₃, where the mass ratio is nearer one.

Our results for mass ratios near one are consistent with the conclusion of Andersen and Sigmund that for energies in the keV range the number of type-j displacements is independent of PKA type. However, for widely different masses this independence only occurs at a much higher energy, a behavior also indicated by the damage energy results of Ref. 3. This difference between our results and those of Andersen and Sigmund is not unexpected because of differences in basic assumptions and because of the approximate solution methods used in Ref. 2.

IV CONCLUSIONS

Although completely general conclusions cannot be drawn from the above results, several observations can be made that are of importance to radiation effects studies. For all the cases

of mass ratio near one

, the fraction of type-J displacement becomes independent of PKA type for $E \geq 4 E_d$. (The absolute value of n_{ij} does depend on the PKA type, with the heavier atom being more efficient in producing displacements). These facts imply that for fast neutron irradiation of such materials the distribution of displacements on the sublattices will depend on the stoichiometry, and on the neutron energy through the relative neutron scattering cross sections of the constituent atoms. For large mass ratios the distribution of displacements will have an additional dependence on the neutron energy, arising because the distribution of displacements on the sublattices does not become independent of PKA type until much higher PKA energies are reached. The total picture of radiation effects in ceramics and insulators must include information on electronic effects as well as displacement effects. However, it seems reasonable to conclude that, based on the results stated above, the question of simulation of fusion reactor damage must include consideration of the material parameters as well as the properties of the radiation source. What is a reasonable simulation environment for one material may not be for another.

Of the various input parameters used in the calculations, the displacement thresholds have the largest effect on the results, with the influence of unequal displacement thresholds on distribution of displacements being very pronounced. In addition to the apparent unequal displacement thresholds in Al_2O_3 already discussed, Crawford et al. [13] have reported measuring three distinct displacement thresholds in $MgAl_2O_4$. There is then a possibility that many materials of interest to the fusion community will fall in the unequal threshold case; and if so, this will have a impact on radiation effects studies.

REFERENCES

- [1] E. M. Baroody, Phys. Rev. 112 (1959) 1571.
- [2] N. Andersen and P. Sigmund, Kgl. Danske Videnskab Selskab, Mat. - fys. Medd. 39, No. 3 (1974).
- [3] Y. Matsutani and S. Ishino, J. Appl. Phys. 48 (1977) 1822.
- [4] D. M. Parkin and C. A. Coulter, Trans. Am. Nucl. Soc. 27 (1977) 318.
- [5] C. A. Coulter and D. M. Parkin, Trans. Am. Nucl. Soc. 27 (1977) 300.
- [6] J. Lindhard, V. Nielsen, M. Scharff and P. V. Thomsen, Kgl. Danske Videnskab. Selskab, Mat. - fys. Medd. 33, No. 10 (1963)
- [7] J. Lindhard, V. Nielsen and M. Scharff, Kgl. Danske Videnskab. Selskab, Mat. - fys. Medd. 36, No. 10 (1969)
- [8] J. Lindhard, M. Scharff and H. E. Schiøtt, Kgl. Danske Videnskab. Selskab, Mat. - fys. Medd. 33, No. 14 (1963).
- [9] Y. Cherr, D. L. Trueblood, O. E. Schow and H. T. Tohver, J. Phys. C 3 (1970) 2501.
- [10] J. V. Sharp and D. Ruinsby, Radiat. Eff. 17 (1973) 65.
- [11] W. D. Compton and G. W. Arnold, Disc. Faraday Soc. 31 (1961) 130.
- [12] D. C. Phillips, AERE Harwell, private communication.
- [13] J. H. Crawford, Jr., K. H. Lee and G. S. White, Bull. Am. Phys. Soc. 23 (1978) 253.

consists of computing the amplitude and phase of the backscattered rays and combining them to determine the backscatter intensity.

Several backscattered rays are illustrated in Fig. 6. Backscattered ray A' arises from an interference between an axial ray reflected from the left side of the sphere and a ray which passes through the sphere and is reflected from the right face of the sphere. This interference can be either constructive or destructive, depending on the optical pathlength through the sphere. Backscattered rays B' and C' are called "glory rays" and arise from rays refracted into the sphere and then internally reflected one or more times. For dielectric spheres with relative refractive indices similar to those of biological cells ($m = 1.01-1.03$), glory rays must undergo two or more internal reflections to contribute to the backscattering (21). Another contribution to the backscattered intensity is from surface waves which cannot be treated by geometrical optics. These waves travel along the surface of the sphere and lose some of their energy by refraction into the sphere. These refracted rays may be reflected internally and contribute to the backscattering.

A biological cell obviously is a much more complicated scattering object than a simple transparent or semitransparent sphere. The measurements presented here are only near backscatter angles ($176^\circ \pm 1^\circ$) and represent the maximum backscattered intensity from a cell as it enters, is immersed, and leaves the laser beam. Nevertheless, these preliminary results indicate that backscattering from particles and biological cells is at least a monotonically increasing function of cell size over a wide range of particle sizes and over a more limited range of cell sizes.

ACKNOWLEDGMENTS

This work was supported in part by the U. S. Energy Research and Development Administration and a grant from The Netherlands Foundation for Medical Research (FUNGO) which is subsidized by The Netherlands Organization for the Advancement of Pure Research (ZWO).

The authors would like to thank Mrs. Elizabeth Sullivan for typing the manuscript and Mrs. Julie Grilly for photographic work.

REFERENCES

1. P. Latimer and B. Tully, Small-angle scattering by yeast cells. A comparison with the Mie predictions. *J. Colloid Interface Sci.* 27, 475 (1968).
2. P. F. Mullaney, M. A. Van Dilla, J. R. Coulter, and P. N. Dean, Cell sizing: A light scattering photometer for rapid volume determination. *Rev. Sci. Instrum.* 40, 1029 (1969).
3. P. F. Mullaney and P. N. Dean, Cell sizing: A small-angle light-scattering method for sizing particles of low relative refractive index. *Appl. Opt.* 8, 2361 (1969).
4. P. F. Mullaney and P. N. Dean, The small-angle light scattering of biological cells, theoretical considerations. *Biophys. J.* 10, 764 (1970).
5. D. J. Arndt-Jovin and T. M. Jovin, Computer-controlled cell (particle) analyzer and separator. Use of light scattering. *FEBS Lett.* 44, 247 (1974).
6. A. L. Koch, Theory of the angular dependence of light scattered by bacteria and similar-sized biological objects. *J. Theor. Biol.* 18, 133 (1968).
7. A. L. Koch and E. Ehrenfeld, The size and shape of bacteria by light scattering measurements. *Biochim. Biophys. Acta* 165, 262 (1968).
8. M. H. Julius, R. G. Sweet, C. G. Fathman, and L. A. Herzenberg, Fluorescence activated cell sorting and its application, In: *Mammalian Cells: Probes and Problems* (C. R. Richmond, D. F. Petersen, P. F. Mullaney, and E. C. Anderson, Eds.), ERDA Symposium Series CONF-731007, Technical Information Center, Oak Ridge, Tenn. (1975), pp. 107-121.
9. M. R. Loken and L. A. Herzenberg, Analysis of cell populations with a fluorescence activated cell sorter. *Ann. N. Y. Acad. Sci.* 254, 263 (1975).

10. L. S. Cram and A. Brunsting, Fluorescence and light scattering measurements on hog cholera-infected PK-15 cells. *Exp. Cell Res.* 78, 209 (1973).
11. R. A. Meyer, S. F. Haase, S. E. Poduiso, and G. M. McKhann, Light scatter patterns of isolated oligodendroglia. *J. Histochem. Cytochem.* 22, 594 (1974).
12. A. Brunsting and P. F. Mullaney, Differential light scattering: A possible method of mammalian cell identification. *J. Colloid Interface Sci.* 39, 492 (1972).
13. R. E. Kopp, J. Lisa, J. Mendelsohn *et al.*, The use of coherent optical processing techniques for automatic screening of cervical cytologic samples. *J. Histochem. Cytochem.* 22, 598 (1974).
14. G. C. Salzman, J. M. Crowell, C. A. Goad *et al.*, A flow-system multiangle light-scattering instrument for cell characterization. *Clin. Chem.* 21, 1297 (1975). J. M. Crowell, B. J. Price, R. D. Hiebert *et al.*, A light scattering system for high-speed cell analysis (1976), manuscript in preparation.
15. G. C. Salzman, J. M. Crowell, J. C. Martin *et al.*, Cell classification by laser light scattering: Identification and separation of unstained leukocytes. *Acta Cytol.* 19, 374 (1975).
16. M. R. Loken, R. G. Sweet, and L. A. Herzenberg, Cell discrimination by multi-angle light scattering. *J. Histochem. Cytochem.* 24, 284 (1976).
17. Recognition Systems, Inc., Van Nuys, California 91406; Model WRD-6420A.
18. On loan from Coulter Electronics, Inc., Hialeah, Florida.
19. Particle Technology, Inc., Los Alamos, New Mexico; now a branch of Coulter Electronics, Inc., Hialeah, Florida.

20. K. Shortman, M. Williams, and P. Adams, The separation of different cell classes from lymphoid organs. V. Simple procedures for the removal of cell debris, damaged cells and erythroid cells from lymphoid cell suspensions. J. Immunol. Meth. 1, 273 (1972).
21. M. Kerker, The scattering of light and other electric radiation. Academic Press, New York (1969), p. 159.

TABLE 1. Mean scattering angle at the center of each ring (parameter) and the polar half-angle subtended by a cell at each ring for a cell-to-detector distance of 30 mm^{*}

Parameter Number	Mean Angle (°)	Polar Half-Angle Subtended (°)
1	0.00	± 0.07
2	0.28	± 0.06
3	0.43	± 0.06
4	0.58	± 0.06
5	0.74	± 0.06
6	0.89	± 0.06
7	1.10	± 0.07
8	1.20	± 0.07
9	1.40	± 0.08
10	1.60	± 0.09
11	1.90	± 0.10
12	2.40	± 0.13
13	3.10	± 0.17
14	3.50	± 0.20
15	4.00	± 0.22
16	4.50	± 0.26
17	5.10	± 0.29
18	5.70	± 0.33
19	6.50	± 0.38
20	7.30	± 0.42
21	8.20	± 0.47
22	9.20	± 0.50
23	10.30	± 0.51
24	11.60	± 0.51
25	12.90	± 0.70
26	14.40	± 0.75
27	176.00	± 1.00

* The angles have been corrected for refraction effects of the 3-mm thick quartz window having an inside face 7 mm from the cell.

TABLE 2. Mean scattered light intensity (channel number) as a function of scattering angle for a series of forward scatter angles and a backscatter angle^{*,**}

Sphere Identification	Size (μm)	C. V. (%)	Angle (°)								
			0.43	0.58	0.74	0.89	1.1	1.2	1.4	1.6	176
5C, black	5	1.1	44	34	41	36	46	53	61	74	68
42C, clear	10	1.3	92	97	130	114	123	131	133	132	89
32C, fluorescent	10	1.3	102	96	133	117	129	136	140	141	101
37C, clear	12.5	1.3	125	122	166	143	150	148	138	122	115
44C, clear	15.7	1.3	145	142	183	154	152	133	101	43	120
38C, purple	19.8	1.2	173	166	206	171	157	115	42	93	126

*The spheres were obtained from Particle Technology, Inc. (19).

**The volume coefficients of variation (C. V.) were taken from the manufacturer's specifications.

TABLE 3. Location of the first diffraction minimum as a function of particle size for the microspheres listed in Table 2

Diameter (μm)	α	θ_{min} ($^{\circ}$)
5	33	6.67
10	66	3.33
12.5	82	2.68
15.7	104	2.11
19.8	131	1.68

Fig. 1. Schematic drawing of the multiangle light-scattering flow system. The beam from a 5-mW helium-neon laser is focused by a spherical lens to a 50- μ m diameter spot at the center of the flow chamber where it intersects the flow stream. A cell passing through the laser beam scatters light onto the forward scatter detector array over a range of angles from 0-14.4° and onto a backscatter detector where $\beta_1 = 2^\circ$ and $\beta_2 = 4^\circ$ so that the backscatter angle is $1.76 \pm 1^\circ$.

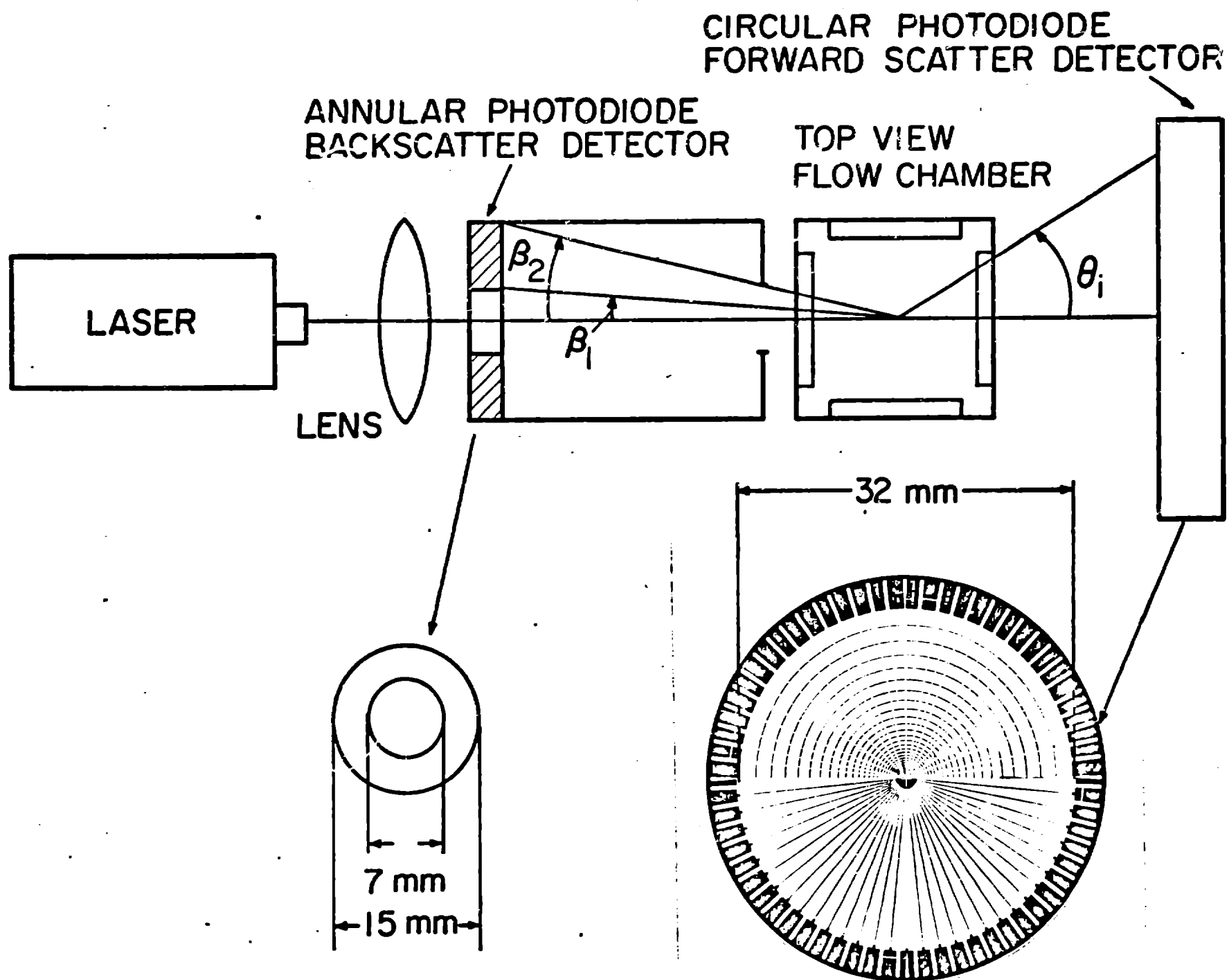


Fig. 2. Clusters of scattered light patterns from a mixture of 10- and 12.5- μm diameter spheres. The 10- μm diameter spheres scatter less light between the parameter numbers 3-6 ($0.43\text{--}0.89^\circ$) where the scattered light intensity is dominated by diffraction.

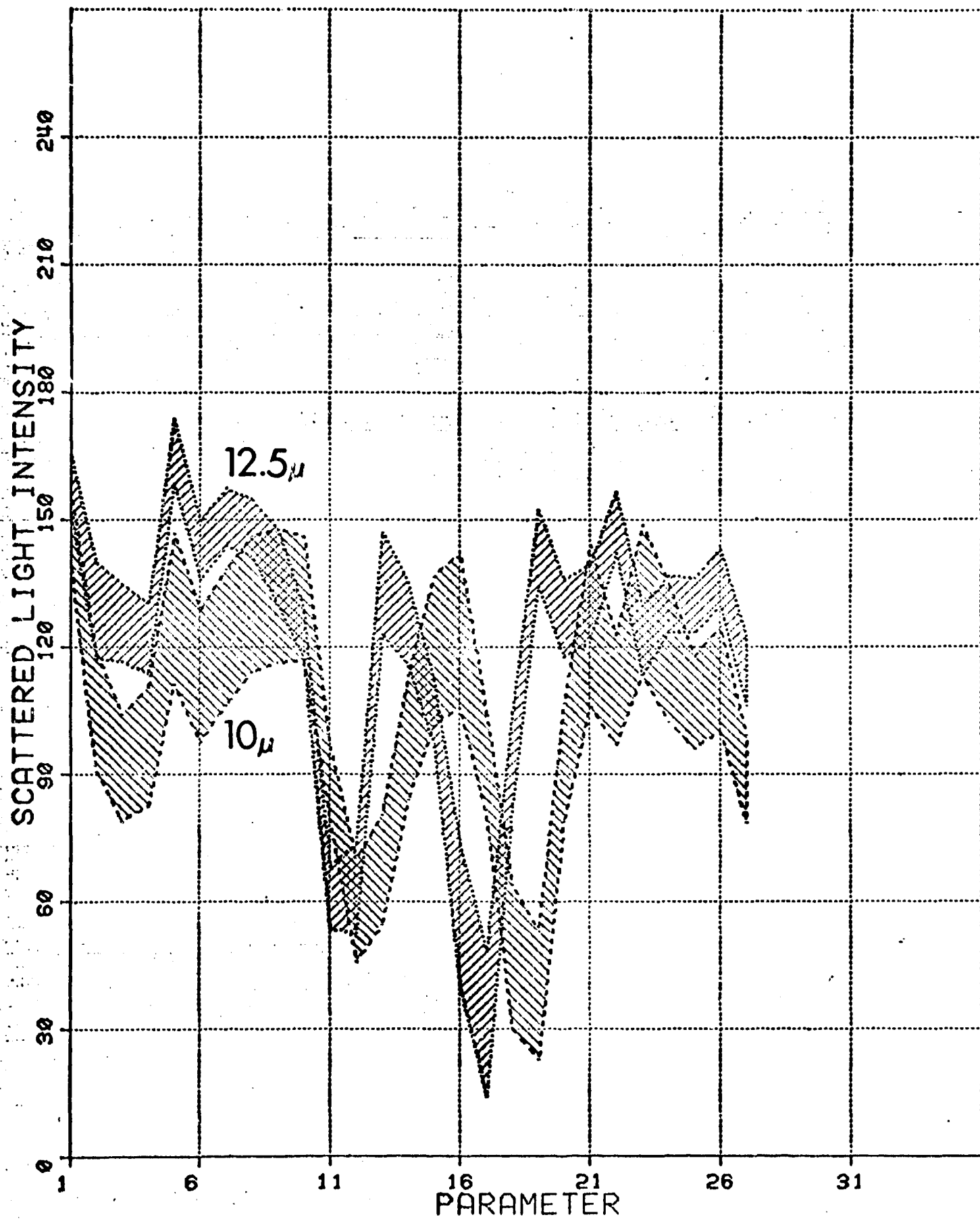


Fig. 3. Pulse-height histograms of number of particles vs scattered light intensity (three decade log scale) for 10- μ m diameter particles (row A) and that for 12.5- μ m particles (row B). Column one is for forward scatter at 1.2°, and column 2 is for backscatter at 176° with respect to the laser beam axis.

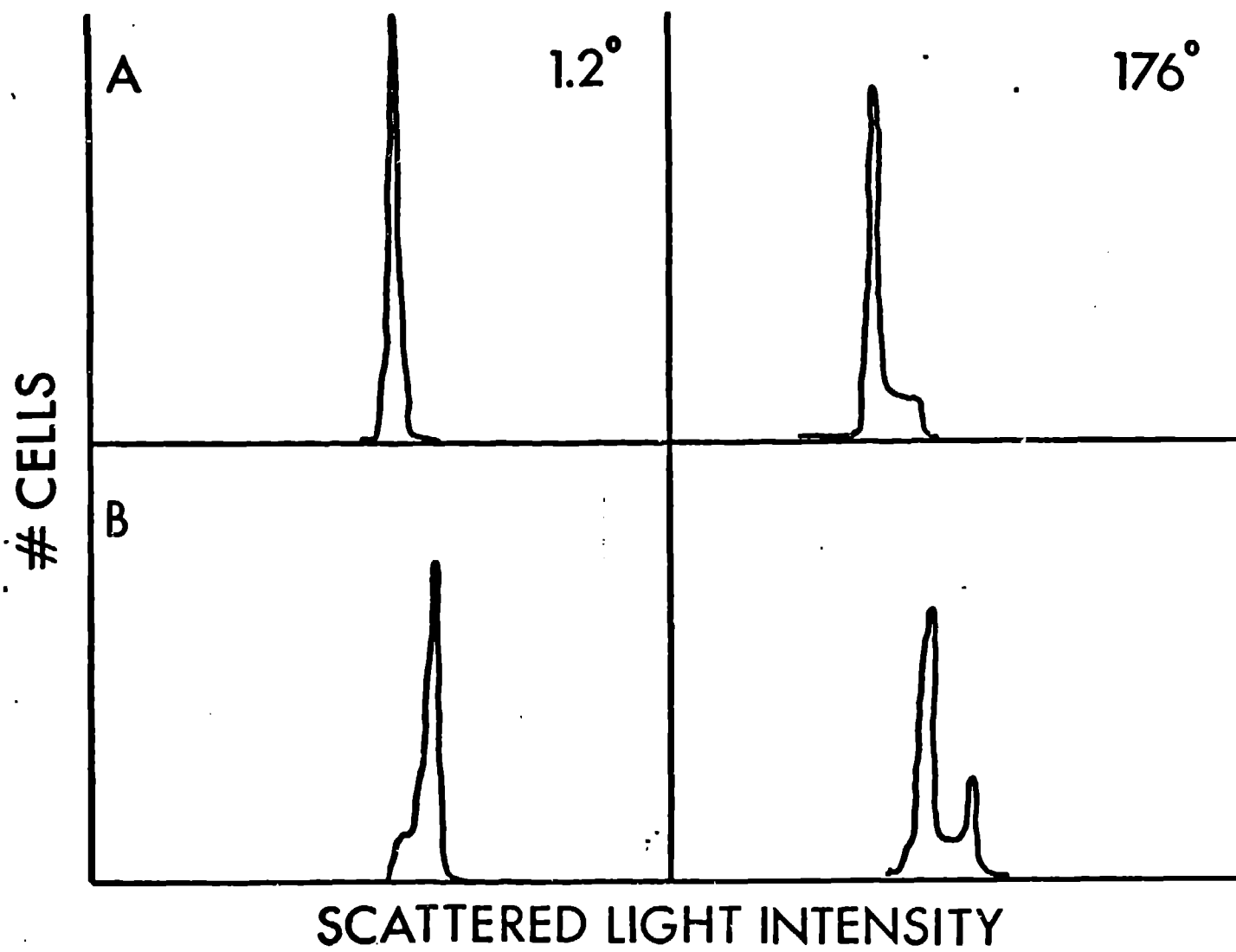
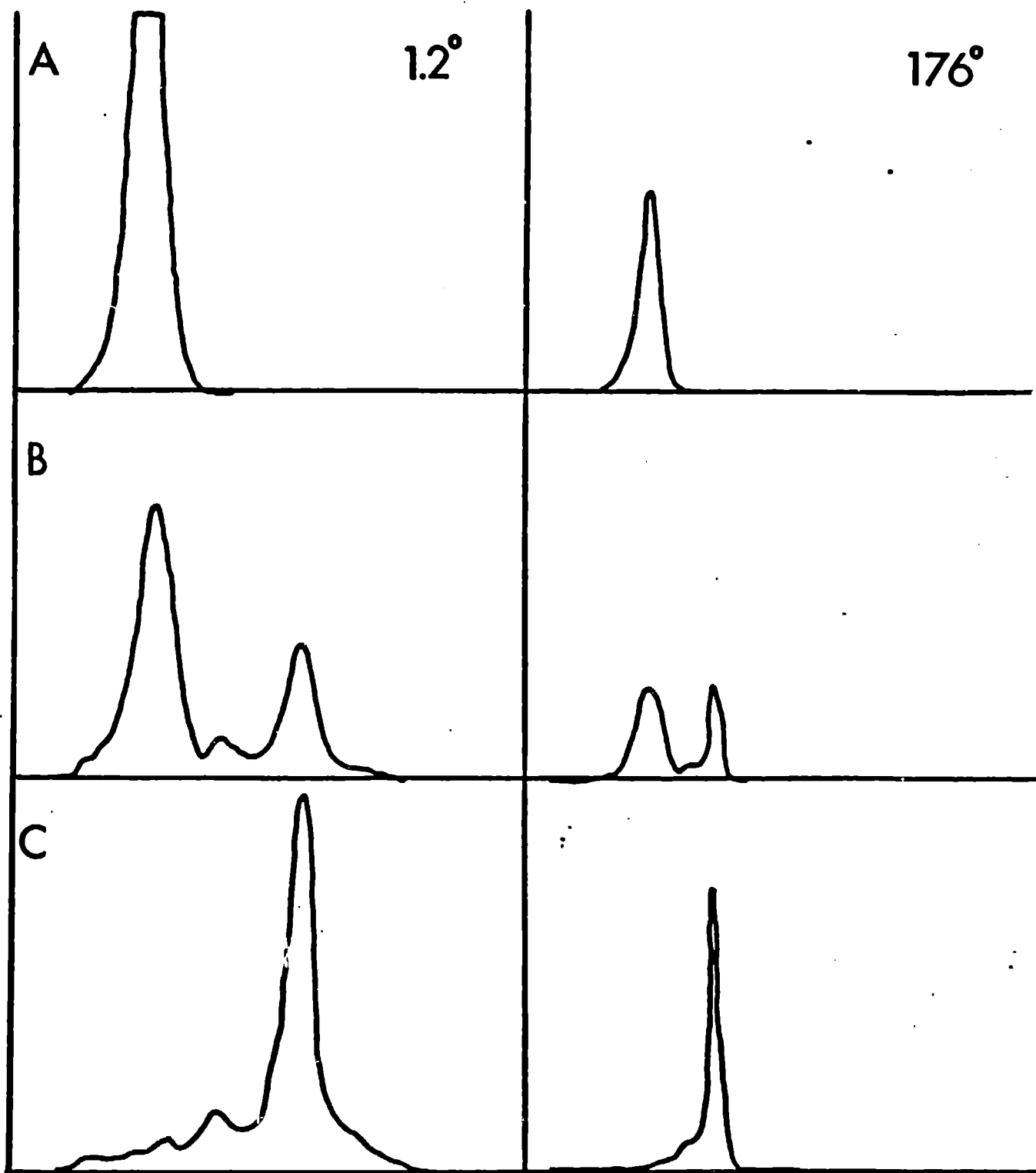


Fig. 4. Forward and backscatter pulse-height histograms of number of cells vs scattered light intensity (three decade log scale): (row A) heparinized mouse peripheral blood; (row B) mouse bone marrow cells; and (row C) mouse bone marrow cells in which the erythrocytes have been lysed with NH_4Cl .



SCATTERED LIGHT INTENSITY

Fig. 5. Collection of pulse-height histograms from mouse bone marrow cells as used for Fig. 4B: I = intensity of scattered light (three decade log scale); θ = scattering angle given in Table 1, and N = number of cells.

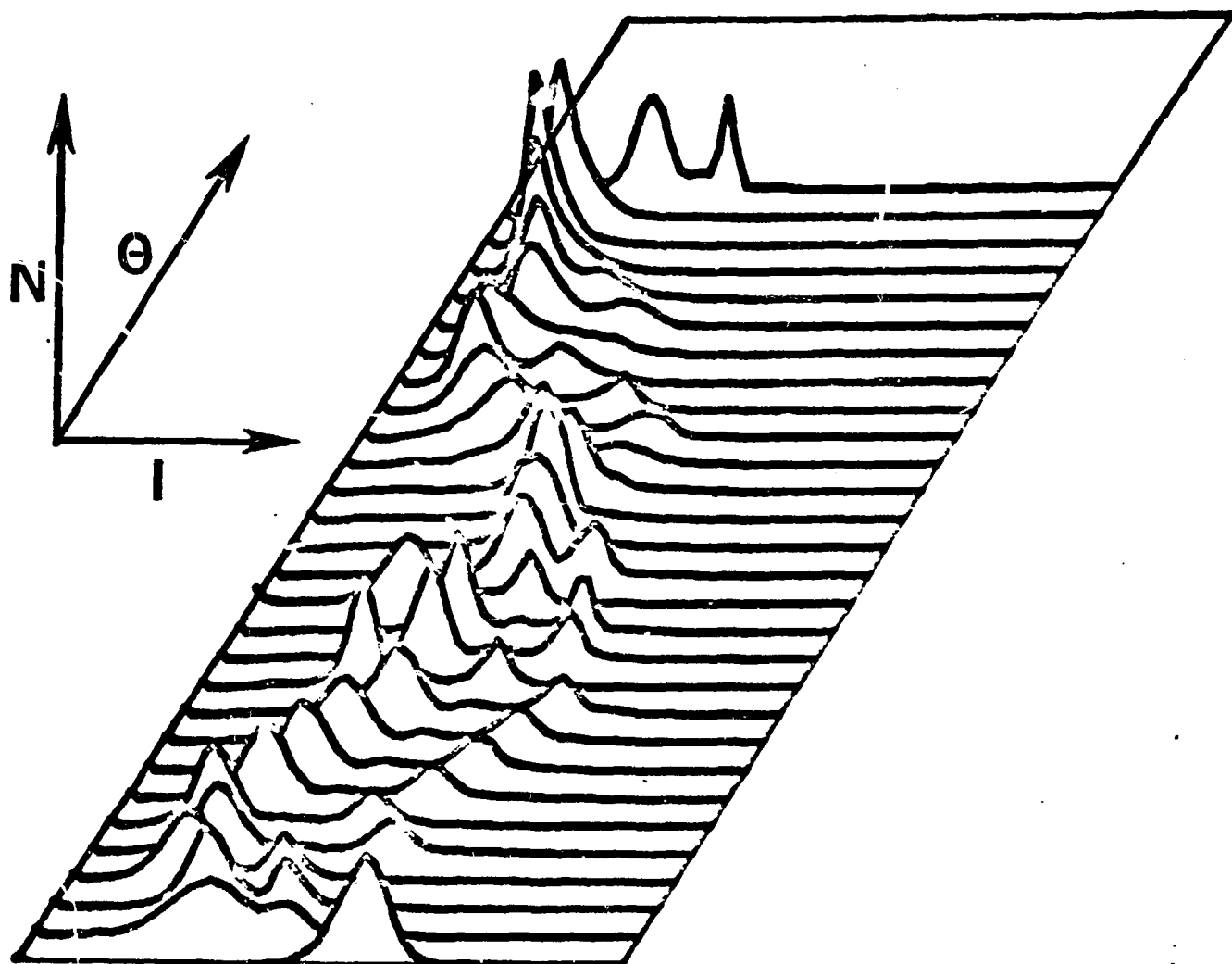


Fig. 6. Tracing of backscattered light rays for a transparent dielectric sphere in which the index of refraction of the sphere is higher than that of the surrounding medium. The unprimed rays are incident light rays, and the primed rays represent those that are backscattered after some number of internal reflections.

